Clays and Clay Minerals, Vol. 24, pp. 297–302. Pergamon Press 1976. Printed in Great Britain

SOLUBILITY DIAGRAMS FOR EXPLAINING ZONE SEQUENCES IN BAUXITE, KAOLIN AND PYROPHYLLITE–DIASPORE DEPOSITS

YOSHIRO TSUZUKI

Department of Earth Sciences, Faculty of Science, Nagoya University, Chikusa-ku, Nagoya, Japan

(*Received* 26 *August* 1974; *and in final form* 25 *July* 1976)

Abstract—Solubility diagrams defined by log $[Al^{3+}]$ and log $[H_4SiO_4]$ are given for hydrous alumina or aluminum silicate minerals which appear in bauxite, kaolin and pyrophyllite–diapore deposits. They are constructed based on thermodynamic data of relevant reactions both at the room temperature and at elevated temperatures.

An aqueous solution reacts to a mineral, in this case K-feldspar, and, by dissolving it, becomes saturated with respect to a certain mineral. This mineral begins to be precipitated and the solution changes its composition as a result of the precipitation as well as further dissolution of the original mineral. Then, it attains saturation with respect to another mineral, which is precipitated thereafter. Thus, different minerals are precipitated in turn.

The sequences of precipitation of minerals can be shown on the diagrams under different conditions. A sequence, aluminum hydroxide → kaolinite or pyrophyllite → silica mineral plus kaolinite or pyrophyllite is expected in a weakly acid solution. In contrast, a sequence, silica mineral → silica mineral plus kaolinite or pyrophyllite is expected in a strongly acid solution. The possibility of application of the sequence of precipitation thus expected to alteration zoning is also discussed.

INTRODUCTION

Bauxite, kaolin, and pyrophyllite–diaspore deposits are formed by weathering or hydrothermal alteration, both of which are caused by aqueous solutions permeating rocks; and zoning of alteration products is a common feature of these deposits.

Solubility diagrams have been proved useful in interpreting natural mineral assemblages or chemical reactions occurring naturally. Log $[Al^{3+}]$ or log $[AlO_2^-]$–pH–log $[H_4SiO_4]$ diagram by Garrels and Christ (1965) and by Curtis and Spears (1971); (pH–$\frac{1}{3}$ pAl^{3+})–pH_4SiO_4 diagram by Kittrick (1969), and log (total dissolved Al)–log (total dissolved Si) diagram by Gardner (1970) are examples.

The writer constructed similar solubility diagrams both at room temperature and at elevated temperatures. In this paper, these diagrams are given and zone sequences expected from them are shown.

SOLUBILITY DIAGRAMS

Construction

Solubility diagrams with coordinates of log $[Al^{3+}]$ and log $[H_4SiO_4]$ were constructed at fixed activities of H^+ and K^+ and at fixed temperatures, and are shown in Figure 1 and Figures 4–9. The following reactions were considered in their construction:

$$KAlSi_3O_8 + 4H^+ + 4H_2O = K^+ + Al^{3+} + 3H_4SiO_4, \quad (1)$$

(K-feldspar(microcline))

$$KAl_3Si_3O_{10}(OH)_2 + 10H^+ = K^+ + 3Al^{3+} + 3H_4SiO_4, \quad (2)$$

(muscovite)

$$Al_2Si_4O_{10}(OH)_2 + 6H^+ + 4H_2O = 2Al^{3+} + 4H_4SiO_4, \quad (3)$$

(pyrophyllite)

$$Al_2Si_2O_5(OH)_4 + 6H^+ = 2Al^{3+} + H_2O + 2H_4SiO_4, \quad (4)$$

(kaolinite)

$$AlO(OH) + 3H^+ = Al^{3+} + 2H_2O, \quad (5)$$

(diaspore)

$$AlO(OH) + 3H^+ = Al^{3+} + 2H_2O, \quad (6)$$

(boehmite)

$$Al(OH)_3 + 3H^+ = Al^{3+} + 3H_2O, \quad (7)$$

((crystalline) gibbsite)

$$SiO_2 + 2H_2O = H_4SiO_4. \quad (8)$$

(α-quartz)

The equilibrium constants of these equations at various temperatures were given by Helgeson (1969) except for (3), (5) and (6), for which they were computed by employing the equations proposed by Helgeson (1969) and the thermodynamic data for pyrophyllite (Haas and Holdaway, 1973), diaspore (Haas, 1972) and boehmite (Barin and Knacke, 1973).

Using the equilibrium constants of the above reactions, the solubility lines on which a solid mineral coexists with solution were drawn for various minerals on each diagram. For reaction (1), as an example, equilibrium constant K_1 is expressed by

$$K_1 = \frac{[K^+][Al^{3+}][H_4SiO_4]^3}{[H^+]^4}, \quad (9)$$

https://doi.org/10.1346/CCMN.1976.0240605 Published online by Cambridge University Press

or

$$\log K_1 = \log [K^+] + \log [Al^{3+}] + 3 \log [H_4SiO_4] - 4 \log [H^+]. \quad (10)$$

If log $[K^+]$ and log $[H^+]$ have fixed values, this equation is represented by a straight line on a log $[Al^{3+}]$ vs. log $[H_4SiO_4]$ diagram. Lines F_1 and F_2 in Figure 1 are such lines.

The solubility line of amorphous silica was drawn after Kennedy (1950), when the solubility of amorphous silica was important.

Although many workers (e.g. Frink and Sawhney, 1967; Parks, 1972; Huang and Keller, 1972) have discussed the state of Al in aqueous solution, dominant species in this study are considered to be Al^{3+}, $Al(OH)^{2+}$ and $Al(OH)_4^-$, following Helgeson (1968) and Helgeson *et al.* (1969). Assuming the activity coefficients of the ions to be unity, the total dissolved Al can be given from the activity of Al^{3+} and the pH using the equilibrium constants of the following equations, and is indicated as the ordinate on the righthand side of the diagrams.

$$Al(OH)_4^- = Al^{3+} + 4OH^-, \quad (11)$$

$$Al(OH)^{2+} = Al^{3+} + OH^-, \quad (12)$$

$$H_2O = H^+ + OH^-. \quad (13)$$

Although H_4SiO_4 dissociates into H^+ and $H_3SiO_4^-$, the ratio of $H_3SiO_4^-$ to H_4SiO_4 is negligibly small in an acid or nearly neutral solution.

Interpretation

Here, the chemical reactions which follow the congruent dissolution of K-feldspar into an aqueous solution are assumed. These reactions at pH = 5, $[K^+] = 0.001$, and temperature = 25°C may be predicted based on the solubility diagram, Figure 1. The dissolution of K-feldspar causes the total concentration of silica, aluminum and potassium in the solution to increase, keeping the relative proportions of 3:1:1. Therefore, the concentration of aluminum and silica produced by the dissolution of K-feldspar should fall on the straight line, I, which passes the point log (total dissolved Al) = 0 ($m_{Al} = 1$) and log $[H_4SiO_4] = 0.477$ ($m_{H_4SiO_4} = 3$) and inclines 45° to the ordinate. As the dissolution of K-feldspar proceeds, the concentration of aluminum and silica change from lower left to upper right along this line, which is called the initial path.

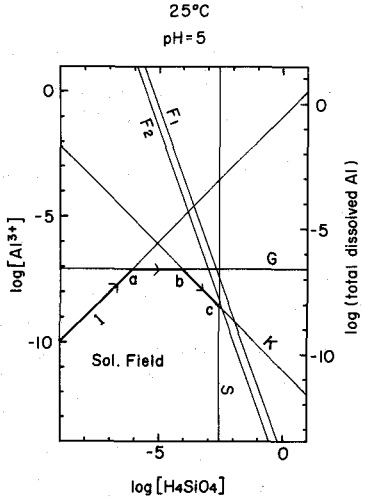

Figure 1. An example of solubility diagrams for K-feldspar alteration. G—gibbsite, K—kaolinite, S—amorphous silica, F_1—K-feldspar (microcline) at $[K^+] = 0.001$, F_2—K-feldspar (microcline) at $[K^+] = 0.01$. I—initial path for K-feldspar dissolution.

When the intial path reaches the gibbsite line at point a, gibbsite begins to be precipitated. The continuing dissolution of K-feldspar brings about the increase of dissolved silica along the gibbsite line, because the precipitation of gibbsite keeps the Al^{3+} concentration constant.

When the path reaches point b, the intersection of the gibbsite and kaolinite lines, gibbsite begins to be dissolved and kaolinite begins to be precipitated. The material balance at this point is expressed by

$$2KAlSi_3O_8 + 4Al(OH)_3 + 2H^+ = 3Al_2Si_2O_5(OH)_4 + 2K^+ + H_2O. \quad (14)$$

After gibbsite is totally consumed, the path turns to the lower right along the kaolinite line, on which the H_4SiO_4 concentration increases with the precipitation of kaolinite.

When the path reaches point c, the intersection of the kaolinite and amorphous silica lines, amorphous silica begins to be precipitated together with kaolinite. The material balance at this point is expressed by

$$2KAlSi_3O_8 + H_2O + 2H^+ = 4SiO_2 + Al_2Si_2O_5(OH)_4 + 2K^+. \quad (15)$$

The path does not proceed further along the silica line. If the path proceeded downward along the silica line, the dissolution of K-feldspar would not take place. Proceeding in this direction means a decrease of the dissolved Al^{3+} without precipitating Al-bearing mineral, which is contradictory to the dissolution of K-feldspar. The reactions occurring in this system are illustrated in Figure 2.

Evaluation of basic assumptions

Before looking at the application of solubility diagrams to zoning, the validity of basic assumptions involved will be examined.

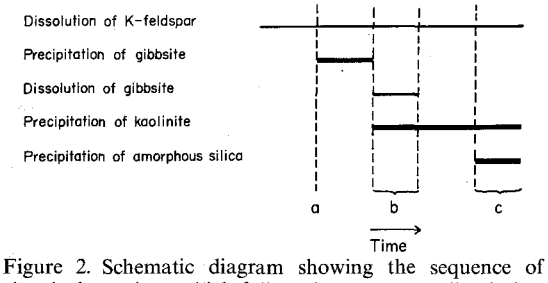

Figure 2. Schematic diagram showing the sequence of chemical reactions which follow the congruent dissolution of K-feldspar at pH = 5, $[K^+] = 0.001$, temperature = 25°C.

https://doi.org/10.1346/CCMN.1976.0240605 Published online by Cambridge University Press

(1) *Thermodynamic data employed.* As mentioned above, the thermodynamic data used for constructing solubility diagrams were derived mainly from Helgeson (1969). For room temperature, more recent data were given by Curtis and Spears (1971), Huang and Keller (1973) and others. These data produce slightly different diagrams, but essential features of the diagrams are not affected.

(2) *Dissolution and precipitation mechanism.* In this study, the dissolution of K-feldspar followed by the precipitation of other minerals is considered instead of the replacement of K-feldspar by other minerals. O'Neil and Taylor (1967), Wilson *et al.* (1971), Keller *et al.* (1971), Nakagawa *et al.* (1973), and Tsuzuki *et al.* (1973, 1974) suggested that the alteration process of a mineral in a solution can be regarded as composed of the dissolution of this mineral, followed by the precipitation of another mineral.

(3) *Congruent dissolution.* The initial stage of the dissolution of K-feldspar may be the exchange reaction of K^+ for H^+ (Wollast, 1967). Experiments by Correns (1961) and Morey and Chen (1955), however, show that K-feldspar is dissolved almost congruently in the main stage.

(4) *Dissolution of K-feldspar.* Natural rocks have, of course, more complex composition than monomineral K-feldspar. If the most soluble mineral in a rock is Na-feldspar instead of K-feldspar, the sequence of reactions shown in Figure 2 remains unchanged, because the positions of the initial path and the solubility lines are the same as in Figure 1. Because these two minerals are widely distributed and liable to be dissolved, the present interpretation of solubility diagrams may be applied to natural zoning in various rocks.

(5) *Partial equilibrium.* In the interpretation of solubility diagrams, the partial equilibrium was assumed following Helgeson (1968) and Helgeson *et al.* (1969). That is, it was assumed that the precipitation of minerals occurs, maintaining equilibrium, while K-feldspar is being dissolved continuously into a solution, i.e. equilibrium is not yet attained. This assumption may be allowed, because the dissolution of K-feldspar is a slow reaction. The incompatible association of K-feldspar and kaolinite is commonly observed in altered granitic rocks (Meyer and Hemley, 1959).

(6) *Change in concentration of* K^+ *and* H^+. Although the solubility diagrams were constructed for fixed K^+ and H^+ concentration, these concentrations vary with the dissolution and precipitation reactions in question. This change in K^+ and H^+ concentration can be estimated quantitatively by the method of Helgeson (1968) and Helgeson *et al.* (1969), but, for the purpose of the present study, a simpler method of estimation is sufficient. The change in pH during the reaction has no important effects on sequences of precipitation, because the mutual relations between the solubility lines of pyrophyllite, kaolinite, diaspore, boehmite and gibbsite are not affected by the change in pH. The effect of changing K^+ concentration can be estimated by drawing solubility lines of K-feldspar and sericite at different K^+ concentrations, like F_1 and F_2 in Figure 1.

At point c in Figure 1, K^+ concentration of the solution increases with the precipitation of amorphous silica and kaolinite and the dissolution of K-feldspar, resulting in a leftward shift of the solubility line of K-feldspar. This line becomes passing point c at the K^+ concentration defined by equation (9); this means that the solution becomes saturated with K-feldspar and the series of reactions described in the previous section terminates leaving an amorphous silica–kaolinite–K-feldspar assemblage behind.

Application to zoning

Natural weathering and hydrothermal alteration take place by the action of migrating aqueous solutions. Therefore, the successive reactions shown in Figure 2 are expected to occur as a function of migration distance as well as that of time. The only difference from Figure 2 is the absence of stage b in which the dissolution of gibbsite and the precipitation of kaolinite occur simultaneously. When the solution becomes saturated with respect to kaolinite, it moves away from where it precipitated gibbsite; therefore, no gibbsite is available for dissolution. Thus, a zoning, dissolution zone → gibbsite zone → kaolinite zone → kaolinite–silica zone → unaltered zone, may be formed. This state is illustrated in the left part of Figure 3.

Continuous flow of the solution will bring about a shift of zone boundary by the following reason. When a new solution reaches the boundary of the dissolution zone and the gibbsite zone, the Al^{3+} concentration is not yet high enough for precipitating gibbsite, because the amount of K-feldspar has decreased by dissolution in the dissolution zone. Therefore, the boundary of these two zones shifts further from the source with time. Other zone boundaries shift likewise, resulting in the migration of zones as illustrated in Figure 3. Accordingly, the mode of

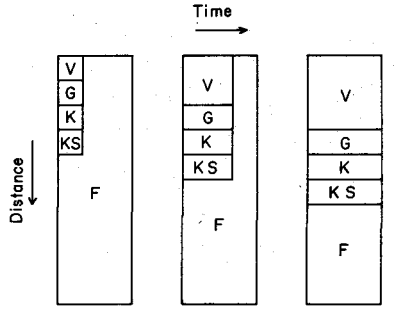

Figure 3. Schematic diagram showing development of zoning pattern under conditions shown in Figure 1. F—feldspar, G—gibbsite, K—kaolinite, S—amorphous silica, V—vacant space.

https://doi.org/10.1346/CCMN.1976.0240605 Published online by Cambridge University Press

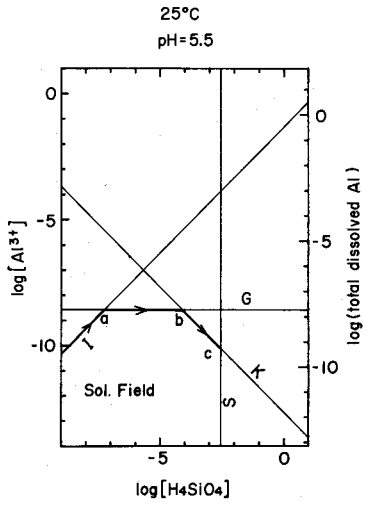

Figure 4. A solubility diagram under weathering conditions. G—gibbsite, K—kaolinite, S—amorphous silica, I—initial path for K-feldspar dissolution.

genesis of a mineral is not uniform; gibbsite, for example, can be formed in either of the following two ways,

(1) K-feldspar → solution → gibbsite,

(2) K-feldspar → solution → kaolinite → solution → gibbsite.

DIAGRAMS FOR VARIOUS CONDITIONS

Diagrams for weathering conditions

For applying zone formation under weathering conditions, the diagrams at 25°C and at a weakly acid pH solution, were prepared. A diagram at 25°C and pH 5.5 is shown in Figure 4. The sequence of precipitation is gibbsite → kaolinite → amorphous silica plus kaolinite. A diagram at 25°C and pH 4 is shown in Figure 5. The sequence is kaolinite → amorphous silica plus kaolinite. A zonal sequence without a gibbsite zone is expected under such low pH conditions.

Diagrams for kaolin and pyrophyllite–diaspore deposits

Interesting zonal sequences similar to hydrothermal deposits, such as kaolin deposits and pyrophyllite–diaspore, were prepared at 200 and 300°C. The minerals concerned are boehmite, kaolinite and amorphous silica at 200°C, and diaspore, pyrophyllite and α-quartz at 300°C.

According to Kennedy (1959), boehmite is formed metastably around 200°C, while diaspore is formed at higher temperatures. Tsuzuki and Mizutani (1969, 1971) showed that kaolinite was transformed into pyrophyllite at 270°C. Mizutani (1966) reported that amorphous silica was formed at a fumarole at 200°C. Examination of solubility diagrams at different pH revealed that there are two different types of sequence of precipitation: (A) sequence from weakly acid solutions and (B) that from strongly acid solutions. Examples of type A are shown on the diagram at 200°C and pH 4 in Figure 6 and that at 300°C and pH 3 in Figure 7. In these diagrams, the initial paths meet the boehmite line or the diaspore line, and the paths turn clockwise similar to the example above. The sequence of precipitation is boehmite → kaolinite → amorphous silica plus kaolinite, or diaspore → pyrophyllite → α-quartz plus pyrophyllite. If $[K^+] = 1.0$ on the diagram in Figure 6, muscovite is precipitated instead of kaolinite. A sericite zone, therefore, may be formed by K^+ rich solution.

If the initial solution is a little more acid, say pH = 2.3, the initial path shifts to the right and first meets the kaolinite line (Figure 8). Boehmite or diaspore zone does not occur in alteration by such solutions.

An example of the type B sequence is shown in the diagram at 200°C and pH 1.8 in Figure 9. In

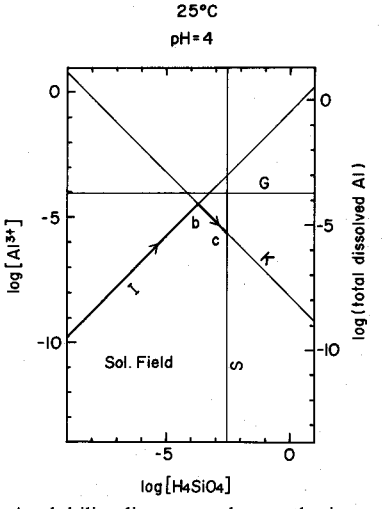

Figure 5. A solubility diagram under weathering conditions. The solution is more acid than in Figure 4. G—gibbsite, K—kaolinite, S—amorphous silica, I—initial path for K-feldspar dissolution.

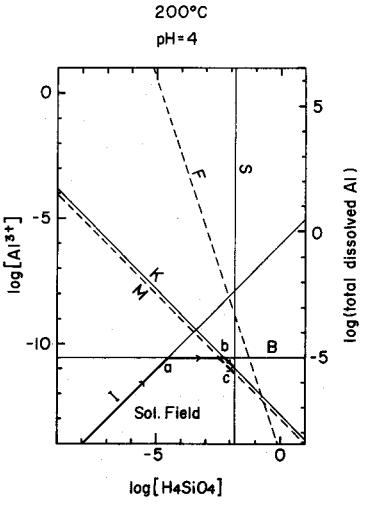

Figure 6. A solubility diagram under hydrothermal conditions. B—boehmite, K—kaolinite, S—amorphous silica, M—muscovite at $[K^+] = 1.0$, F—K-feldspar at $[K^+] = 1.0$, I—initial path for K-feldspar dissolution.

https://doi.org/10.1346/CCMN.1976.0240605 Published online by Cambridge University Press

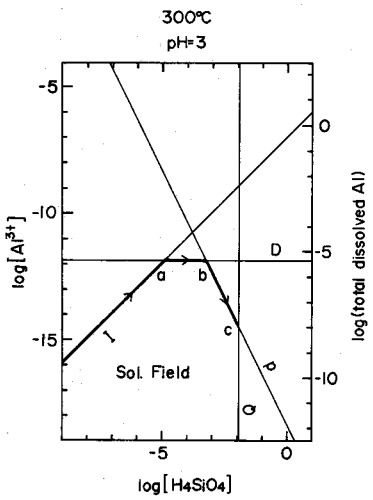

Figure 7. A solubility diagram under hydrothermal conditions. D—diaspore, P—pyrophyllite, Q—α-quartz, I—initial path for K-feldspar dissolution.

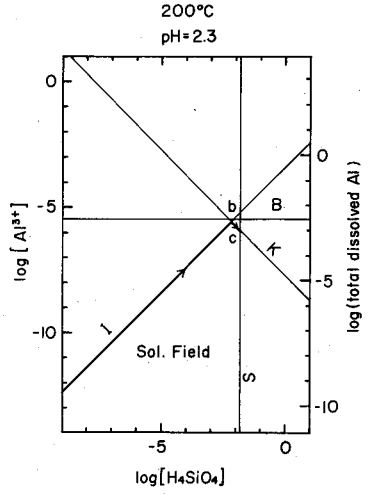

Figure 8. A solubility diagram under hydrothermal conditions. B—boehmite, K—kaolinite, S—amorphous silica, I—initial path for K-feldspar dissolution.

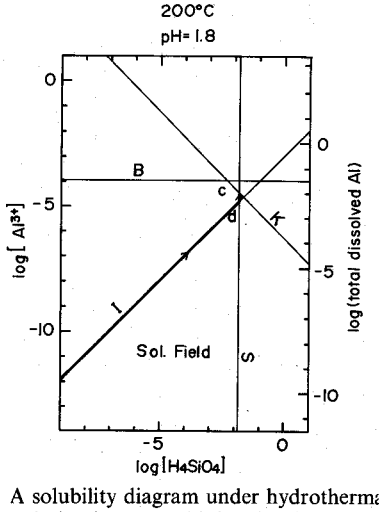

Figure 9. A solubility diagram under hydrothermal conditions. The solution is more acid than in Figure 6. B—boehmite, K—kaolinite, S—amorphous silica, I—initial path for K-feldspar dissolution.

this diagram, the initial path first meets the amorphous silica line at point d, and then the solution changes its composition upward along this line, precipitating amorphous silica. Thus the direction is anticlockwise. When the path reaches point c, kaolinite begins to be precipitated together with amorphous silica. Consequently, the sequence expected is silica → silica plus kaolinite.

Acknowledgements—The author is grateful to Dr. W. H. Huang of University of South Florida for reading the manuscript and making many helpful comments. He is indebted to Dr. K. Nagasawa of Nagoya University for encouraging support, helpful suggestions and critical comments. He also wishes to express his thanks to Dr. N. Nakai and Dr. S. Mizutani of Nagoya University for their constructive suggestions.

REFERENCES

Barin, I. and Knacke, O. (1973) *Thermochemical Properties of Inorganic Substances*: Springer, Berlin.

Correns, C. W. (1961) The experimental chemical weathering of silicates: *Clay Min. Bull.* **4,** 249–265.

Curtis, C. D. and Spears, D. A. (1971) Diagenetic development of kaolinite: *Clays & Clay Minerals* **19,** 219–227.

Frink, C. R. and Sawhney, B. L. (1967) Neutralization of dilute aqueous aluminum salt solutions: *Soil Sci.* **103,** 144–148.

Gardner, L. R. (1970) A chemical model for the origin of gibbsite from kaolinite: *Am. Mineralogist* **55,** 1380–1389.

Garrels, R. M. and Christ, C. L. (1965) *Solutions, Minerals, and Equilibria*: Harper & Row, New York.

Haas, H. (1972) Diaspore–corundum equilibrium determined by epitaxis of diaspore on corundum: *Am. Mineralogist* **57,** 1375–1385.

Haas, H. and Holdaway, M. J. (1973) Equilibria in the system Al_2O_3–SiO_2–H_2O involving the stability limits of pyrophyllite, and thermodynamic data of pyrophyllite: *Am. J. Sci.* **273,** 449–464.

Helgeson, H. C. (1968) Evaluation of irreversible reactions in geochemical processes involving minerals and aqueous solutions—I. Thermodynamic reactions: *Geochim. Cosmochim. Acta* **32,** 853–877.

Helgeson, H. C.. (1969) Thermodynamics of hydrothermal systems at elevated temperatures and pressures: *Am. J. Sci.* **267,** 729–804.

Helgeson, H. C., Garrels, R. M. and Mackenzie, F. T. (1969) Evaluation of irreversible reactions in geochemical processes involving minerals and aqueous solutions—II. Applications: *Geochim. Cosmochim. Acta* **33,** 455–481.

Huang, W. H. and Keller, W. D. (1972) Geochemical mechanics for the dissolution, transport, and deposition of aluminum in the zone of weathering: *Clays & Clay Minerals* **20,** 69–74.

Huang, W. H. and Keller, W. D. (1973) Gibbs free energies of formation calculated from dissolution data using specific mineral analyses. III. Clay Minerals: *Am. Mineralogist* **58,** 1023–1028.

Keller, W. D., Hanson, R. F., Huang, W. H. and Cervantes, A. (1971) Sequential active alteration of rhyolitic volcanic rock to endellite and precursor phase of it at a spring in Michoacan, Mexico: *Clays & Clay Minerals* **19,** 121–127.

Kennedy, G. C. (1950) A portion of the system silica–water: *Econ. Geol.* **45,** 629–653.

Kennedy, G. C. (1959) Phase relations in the system Al_2O_3–H_2O at high temperatures and pressures: *Am. J. Sci.* **257,** 563–573.

https://doi.org/10.1346/CCMN.1976.0240605 Published online by Cambridge University Press

Kittrick, J. A. (1969) Soil minerals in the Al_2O_3–SiO_2–H_2O system and a theory of their formation: *Clays & Clay Minerals* **17,** 157–167.

Meyer, C. and Hemley, J. (1959) Hydrothermal alteration in some granodiorites: *Clays & Clay Minerals* **6,** 89–100.

Mizutani, S. (1966) Transformation of silica under hydrothermal conditions: *J. Earth Sci.* **14,** 56–88.

Morey, G. W. and Chen, W. T. (1955) The action of hot water on some feldspars: *Am. Mineralogist* **40,** 996–1000.

Nakagawa, Z., Hatahira, S., Urabe, K. and Yamada, H. (1973) Studies on the crystallization process in the system feldspar–NaOH–H_2O at low temperatures (in Japanese): *J. Japan. Assoc. Mineral. Petrol. Econ. Geol.* **68,** 58–69.

O'Neil, J. R. and Taylor, H. P., Jr. (1967) The oxygen isotope and cation exchange chemistry of feldspars: *Am. Mineralogist* **52,** 1414–1437.

Parks, G. A. (1972) Free energies of formation and aqueous solubilities of aluminum hydroxides and oxide hydroxides at 25°C: *Am. Mineralogist* **57,** 1163–1189.

Tsuzuki, Y. and Mizutani, S. (1969) Kinetics of hydrothermal alteration of sericite and its application to the study of alteration zoning: *Proc. Intern. Clay Conf.* 1969 **1,** 513–522.

Tsuzuki, Y. and Mizutani, S. (1971) A study of rock atteration process based on kinetics of hydrothermal experiment: *Contr. Mineral. Petrol.* **30,** 15–33.

Tsuzuki, Y., Mizutani, S., Shimizu, H. and Hayashi, H. (1973) Kinetics of alteration of K-feldspar to kaolinite and its application to the genesis of kaolin deposits: *Proc. Intern. Clay Conf.* 1972, 313–319.

Tsuzuki, Y., Mizutani, S., Shimizu, H. and Hayashi, H. (1974) Kineties of alteration of K-feldspar and its application to atteration zoning: *Geochem. J.* **8,** 1–20.

Wilson, M. J., Bain, D. C. and Mchardy, M. J. (1971) Clay mineral formation in a deeply weathered boulder conglomerate in north-east Scotland: *Clays & Clay Minerals* **19,** 345–352.

Wollast, R. (1967) Kinetics of the alteration of K-feldspar in buffered solution at low temperature: *Geochim. Cosmochim. Acta* **31,** 635–648.

https://doi.org/10.1346/CCMN.1976.0240605 Published online by Cambridge University Press